International Journal of Sciences: Basic and Applied Research (IJSBAR)

ISSN 2307-4531
(Print & Online)

http://gssrr.org/index.php?journal=JournalOfBasicAndApplied

Pore and Grain Geometry Analysis of Sandstone Reservoir Rocks from a Well of a Northern German Basin

Kim Phuong Lieu [a*], W. Altermann [b], T. Drobek [c], M. Frei [d], R.W. Stark [e].

[a] *Petrography – Sedimentology Laboratory, Analysis Laboratory Center, Vietnam Petroleum Institute (VPI). Block G1 Thanh Da Hotel, Binh Thanh District, Ho Chi Minh City, Vietnam*

[b] *Department of Geology, University of Pretoria 0002 Pretoria, RSA*

[c] *TU Darmstadt Energy Center, Technische Universität Darmstadt, Petersenstr. 13, D-64287 Darmstadt, Germany*

[d] *University of Munich, Department of Earth and Environmental Sciences, Luisenstr.37, D-80333 Munich, Germany*

[e] *Centre of Smart Interfaces and Department of Materials and Geosciences, Technische Universität, Petersenstr. 32, D-64287 Darmstadt, Germany*

[a] *Email: phuonglk@vpi.pvn.vn*

Abstract

Pore space and grain geometry are important physical properties distinguished in reservoir rocks, particularly in sandstones, due to their influence on oil and gas reservoir quality. Therefore, a detailed study of pore space morphology and grain surface roughness in sandstone reservoir rocks is a key element in petroleum geology. It is eminent in understanding of the adhesion of hydrocarbons in rocks and coupled fluid flows in pores and along grain surfaces.

In this work, sandstone samples taken from a well of a Northern German basin deposit have been analysed by thin section petrography, Confocal Raman Microscopy and Confocal Laser Scanning Microscopy (CLSM). The roughness of grain surfaces is analysed and the pore geometries of sandstone rocks are verified. Roughness and pore geometry have a significant impact on the wetting behaviour and adhesion properties of hydrocarbon fluids, water or carbon dioxide (CO_2) to the pore walls.

---

*Corresponding author.

The results show the relationship between the composition of sandstones and their pore geometry and the grain surface roughness. The geometry of the pore morphology and the grain surface shows a range from very rough to flat smooth crystal facets, from few hundreds to sub-micron, depending on the scale of observation. The 50x and 100x magnifications were applied in this study. The findings offer a detailed insight into the relationship of pore space morphology and the grain surface roughness. The results add important parameters to the calculation models for hydrocarbon exploitation and to enhancement of the amount of oil recovery.

Keywords: reservoir rock; pore geometry; sandstones; confocal laser scanning microscope; enhanced oil recovery; petroleum geology.

1. Introduction

In sandstone reservoir rocks the porosity plays an important role because it relates to the total capacity of hydrocarbon reserves of sandstones. In addition, the grain surface roughness is an essential factor of reservoir quality as it controls the pore surface and the pore shape complexity. Therefore, a large influence on the hydrocarbon exploitation capacity is related to pore space morphology and adhesion of hydrocarbons to grain surfaces. The significant hydrocarbon volume is held in pore spaces and adhered on grain surfaces. This is a major factor leading to the loss of high percentage of hydrocarbon volume in the exploitation. Therefore, detailed investigations of the pore morphology and of the grain surface roughness not only reveal the fine structures insight pore spaces of rocks, but also allow to estimate the amount of reserved and exploitable oil in reservoir rocks via models.

The variation of the pore shape and the grain morphology is directly influenced by diagenetic processes like, re-orientation of grains during compaction, dissolution and simultaneous or subsequent replacement by authigenic minerals, which are precipitated or recrystallised during the diagenisis in depositional settings. The morphology of pore spaces depends on the grain size distribution, the shape of grains, packing and cementing, while the grain surface roughness is influenced by mineralogical and transportation parameters and the overgrowth by authigenic minerals. The pore geometry and the grain surfaces are usually altered during lithification, beginning with compaction and cementing of loose sediment grains and, finally, conversion into a solid rock.

The quantitative characterisation of the roughness of particles/grains of detrital sediments and their pore morphology, has been the subject in many studies. Various techniques have been developped to this end such as e.g. the harmonic wavelet descriptors (HWD) that act as a mathematical microscope based method of the harmonic wavelet transform. The descriptors analyse structures of a grain appearing at different scales of resolution. Lower resolution levels represent the coarse aspects of the grain contour, while the higher resolution levels represent its increasingly fine structures [1, 2]. Pore morphology and pore surface roughness in rocks have been investigated using small-angle neutron scattering (SANS) and ultra-small angle neutron scattering (USANS) [3, 4, 5]. Also, confocal laser scanning microscope techniques can be applied to measure roughness and pore geometry. The authors in reference [6] performed 3-D geometry of the pore system of the Fontainebleau sandstone with different degrees of cementation and diagenesis, and the authors in reference [7] analysed the fracture surface roughness of granite.

The authors in reference [8] measured the microscopic three dimensional distributions of pore bodies and pore throats in sandstones with hydrocarbon reservoir potential. The authors in [9] also used a confocal laser scanning microscope to verify the three-dimensional pore of the Fontainebleau sandstone.

In this study, the pore morphology and the sediment grain roughness have been analysed with the CLSM at various magnifications: 50x, 100x. From the data we calculated profiles, 3-D reconstructions, and root mean square roughness parameter to correlate the numerical values with the petrographic description. The pore space morphology of the investigated sandstone reservoir rocks is characterised by the features of the clastic grains, with rounded to well-rounded and sub-spheroidal and elongate shapes and grain sizes ranging from fine to medium. The clastic grains are arranged in the rhombohedral type, commonly forming triangular pore spaces and are cemented in the early phase, by the precipitation of calcite cements, present in most pore spaces. The sediment grain surfaces vary due to overgrowth by authigenic minerals, formed during diagenesis and leading to very rough grain surfaces. Different types of pore morphology and grain surfaces were observed, ranging from very rough, fractal-like surfaces to flat, smooth crystal facets.

2. Samples and methods

Selected sandstone samples were taken from core plugs derived from sandstone reservoir rocks of a well of the Northern German basin at a depth of approximately 5000 m. Thin sections of the samples were studied with a Leica DM 2500M petrographic microscope. Parts of the samples were separated into individual grains and small grain groups and mounted on top of a conical sample holder. Then the composition of these grains was characterised with a confocal Raman microscope (alpha300R; WITecGmbH, Ulm, Germany). Raman data were processed with WITec Project software. The grain surface roughness and the pore morphology were conducted with a digital confocal laser scanning microscope (CLSM, VK-8700) with a red laser (658 nm).

The CLSM delivers digitally sandwiched surface images of the sample, with high depth of focus and quantitative topography for each layer. Two different objectives were used for data acquisition: 50x and 100x. This corresponds to a scan size of 140 μm x 105 μm and 70 μm x 50 μm, respectively. The image size was 1280 x 1024 pixels. The resolution in z direction was 0.5 μm which was the mean distance between two adjacent layers. From the digital data set the root mean square roughness parameter (R_q) was calculated and the morphology of the pores was evaluated from 3D and profile images. To calculate the root mean square roughness on the nanometre scale the background waviness was removed. After an automatic plane tilt correction, the images were flattened subtracting an appropriate sphere to correct for a spherical surface. The R_q parameter was calculated for all images at 50x and 100x magnifications, following the formula below (*VK Analyzer. Ver. 2.3 Formanalyse software*). The root mean square R_q of the height of each point in the region of interest, is expressed as

$$R_q = \sqrt{\frac{1}{N}\sum_{n=1}^{N} Z_n^2}$$

Here. Z_n indicates the height of each point of the reference surface. N is the number of measured points. The reference surface is defined as a plane at the average height of the filtered data.

3. Results

3.1. Petrography

The three studied samples were fine to medium grained sandstones and have moderate to very good sorting. The grains were round to very round (figure 1.1 and 1.2), sometimes sub-rounded (figure 1.3) and the grain shape is commonly subspheroidal and elongate. In figure 1.3, the pores stained blue were formed by an open network. The intergranular pores occupied a high volume (15%). The pores displayed in figures 1.1 and 1.2 are filled mainly by calcite and clay cement, and sometimes show quartz overgrowth thus, the porosity is poor (5%-8%). Quartz grains (Q) with shiny, pale, reddish brown colour were the major components of the three samples, which contain a varying amount of other detrital particles such as weathered and dissolved alkaline feldspar (K-F), plagioclase grains and rock fragments (R-F).

The three samples displayed a complicated polystage diagenesis. Primarily, under pressure, the grains were partly corroded at grain boundaries (figure 1.2) and dissolved forming intragranular pores (figure 1.1 and 1.3), along with the precipitation and formation of cements of illite-chlorite minerals (IC) and/or haematite skins, coating the grains (figure 1.1 and 1.2). Subsequently, the precipitation of quartz cements (Qc) in pore spaces and overgrowth by quartz (Qz) along the pore boundaries occurred (figure 1.1). The last generation was the precipitation of calcite cements in pore spaces (figure 1.1 and 1.2).

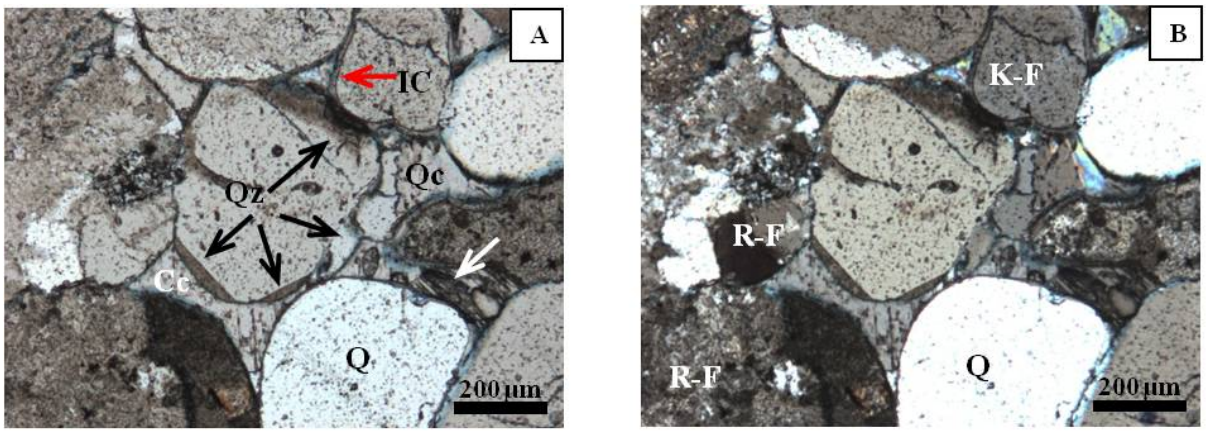

Figure 1.1: Illite-chlorite grain coatings (IC), syntaxial quartz overgrowth (Qz) on detrital quartz. Pore spaces are filled by calcite cement (Cc) and sometimes quartz cement (Qc). In the right picture (A), the arrow points to dissolved feldspar, forming micro pores within feldspar.

Figure 1: Petrographic microscope images of samples RL I_2111, RL I_4146 and RL I_5041 corresponding to Figure 1.1, figure 1.2 and figure 1.3 with plane polarised (A) and crossed polars (B).

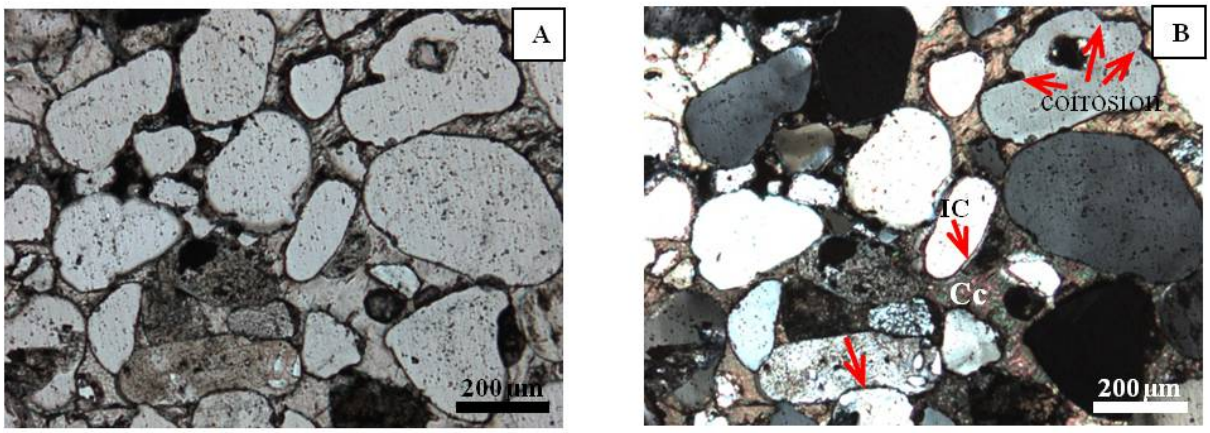

Figure 1.2: Illite-chlorite grain coatings (IC, bright), grain contacts are saturated (arrow) and pore-filling is calcite cement (Cc). Detrital grains are corroded.

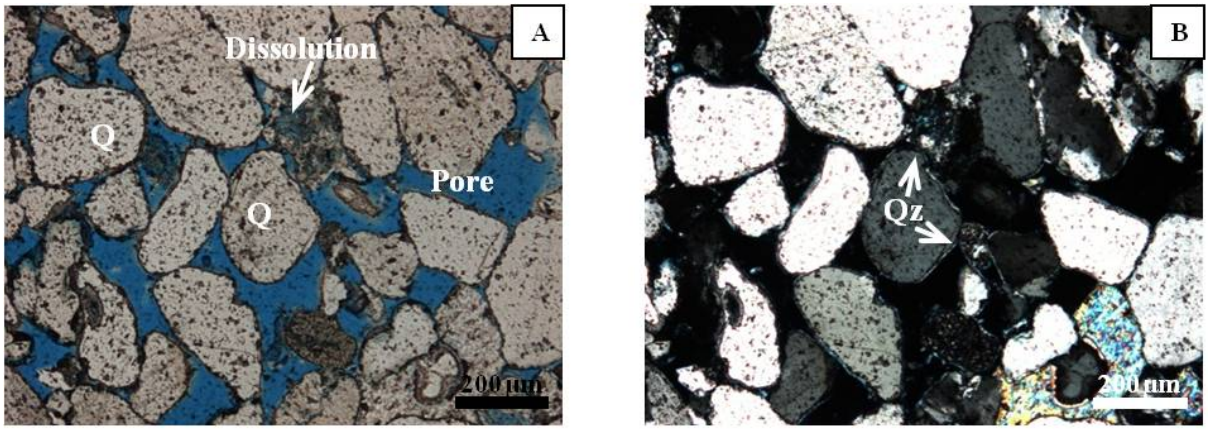

Figure 1.3: Open pores are stained blue and authigenic quartz overgrowth (Qz) on detrital grains. The arrow points to micro pores due to detrital grain dissolution.

3.2. Grain roughness measurements

The grain surface displayed various roughness levels, dependant on the scale of observation, at 50x or 100x magnification. In this CLSM investigations the results for a characteristic quartz grain surface roughness analysis showed that the texture and morphology of the quartz grain surface were altered during diagenesis due to compaction, cementation and the overgrowth by authigenic minerals.

Figure 2 is an image of the quartz grain surface of sample RL I_2111. The quartz composition was verified by confocal Raman spectroscopy analysis (figure 2.1B). The quartz surface in figure 2.1 with dark gray colour is below that with white colour which is overgrown by authigenic minerals. However, the authigenic mineral coating cannot be confirmed by confocal Raman spectroscopy, because the concentration of the authigenic mineral is very low compared to the quartz. The Raman band intensity of the authigenic mineral is obscured by the quartz signal. As observed in CLSM image (figure 2.2) the quartz surface is very rough due to overgrowth by the authigenic minerals which form deep troughs and peaks (arrow marks).

The roughness of this quartz surface is evidenced by the root mean square, calculated for the entire image (figure 2.2A) with R_q: 2.52 µm. Additionally, the rough quartz surface was analysed along the line profile (figure 2.3B). The amplitude of this profile is quite rough with the presence of many high peaks and low valleys. The difference between the highest spike and lowest pit is 11.1 µm (figure 2.3B).

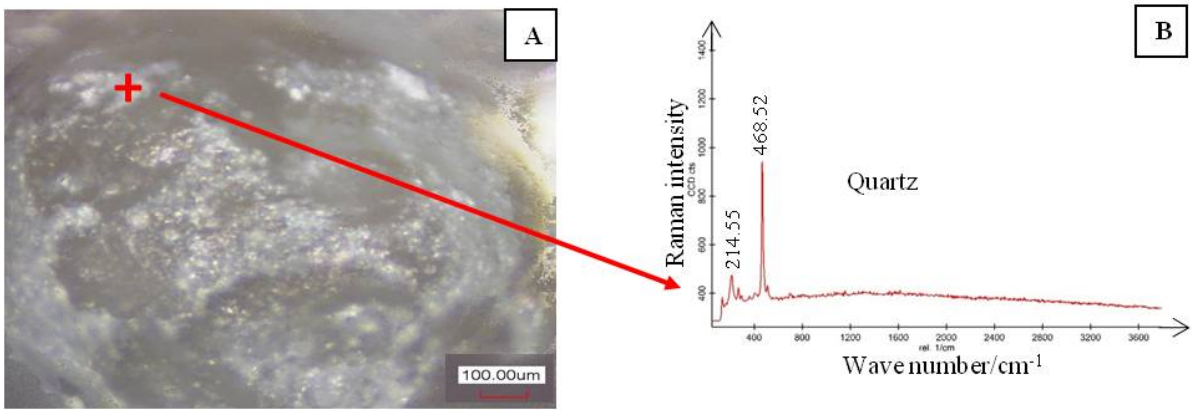

Figure 2.1: Overview image of quartz grain and Raman spectrum.

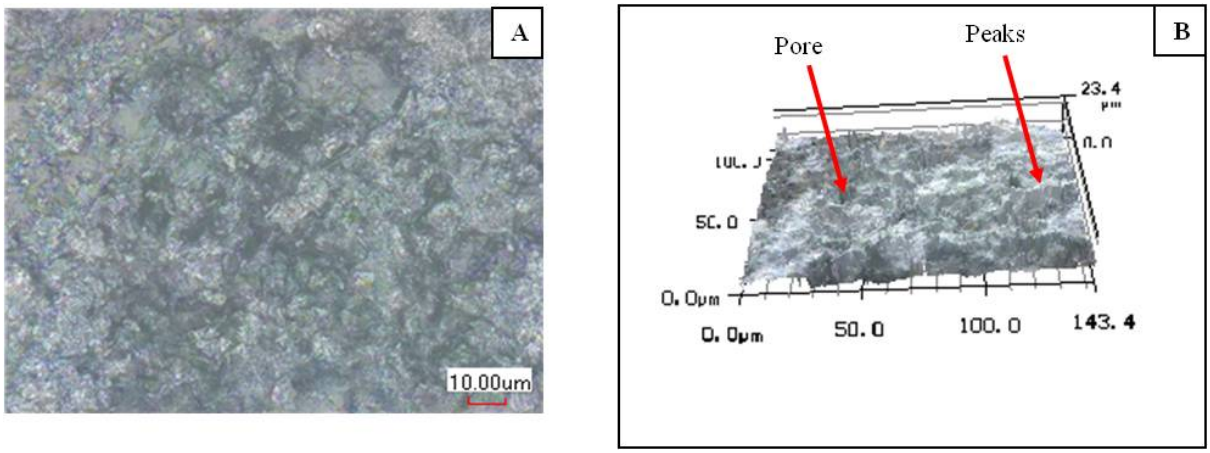

Figure 2.2: CLSM image of the quartz surface taken at 100x magnification.

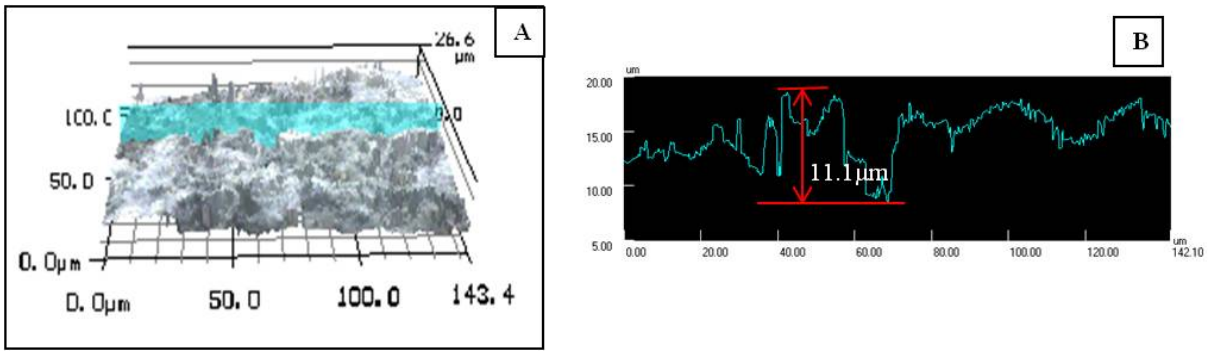

Figure 2.3: 3-D image and line profile of the quartz surface taken at 100x magnification.

The grain topography affected by diagenesis is illustrated in figure 3, the quartz grain of the sample RL I_4146 is compacted at a grain contact area in the left of figure 3.1A and is overgrown by calcite as well, as analysed by the Raman spectrum in figure 3.1B. The compacted grain contact area and overgrowth of calcite, which form the rough quartz surface with low and high positions, are magnified and can be seen clearly in figure 3.2. The arrows point to calcite overgrowth, compacted area and real quartz surface in figure 3.2B. The roughness of the quartz surface is shown by the profile in figure 3.3B. The line profile is rather smooth for the original quartz surface, while the high peaks in the profile are only present in the calcite overgrown area and low valleys at compacted area (arrow marks). The roughness of the entire quartz surface, at 100x magnification in figure 3.2A is calculated and shows a roughness parameter of R_q 3.59 µm.

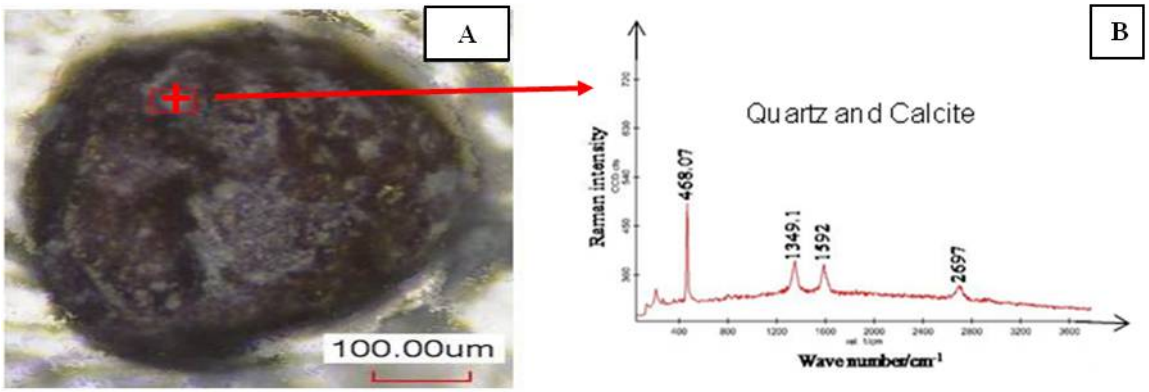

Figure 3.1: Overview image of quartz grain at 5x magnification and Raman spectrum.

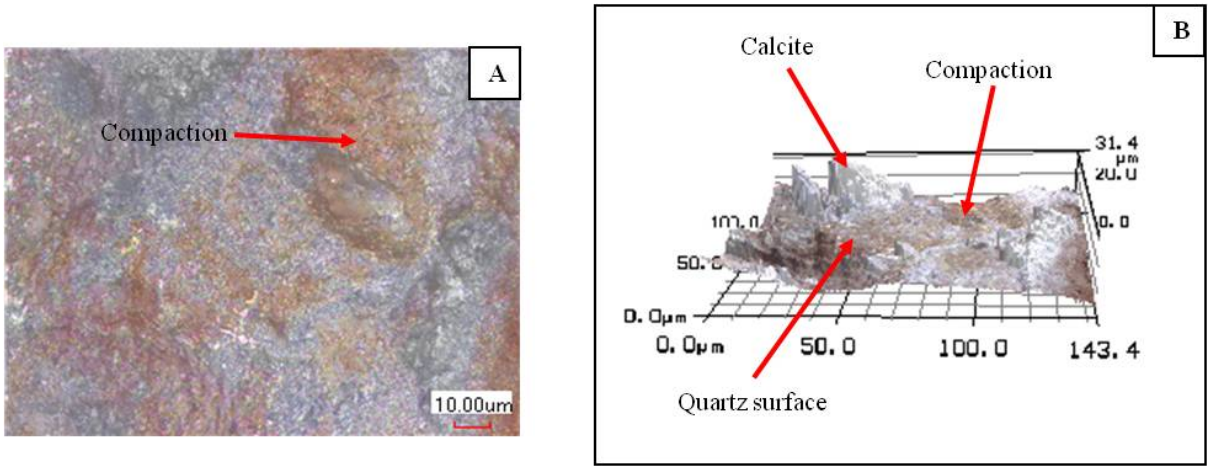

Figure 3.2: CLSM image of the quartz surface taken at 100x magnification.

Figure 4, shows the surface of a grain of sample RL I_5041. The Raman spectrum of the quartz grain is shown in figure 4.1B. As shown in figure 4.1A, the quartz surface was quite smooth with tiny pits due to collisions with other grains during transport or dissolution in diagenesis. This quartz surface was only slightly altered during diagenesis and probably was an original surface. Partially, the original quartz surface was covered by authigenic cement minerals with white colour, as pointed out by arrow mark in figure 4.2B. The calculated root mean square parameter is 1.57 µm.

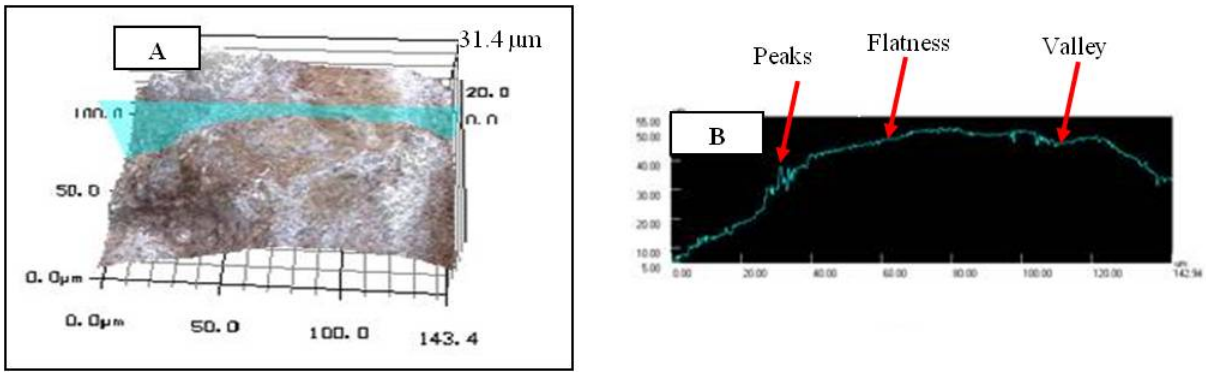

Figure 3.3: 3-D image and line profile of the quartz surface taken at 100x magnification.

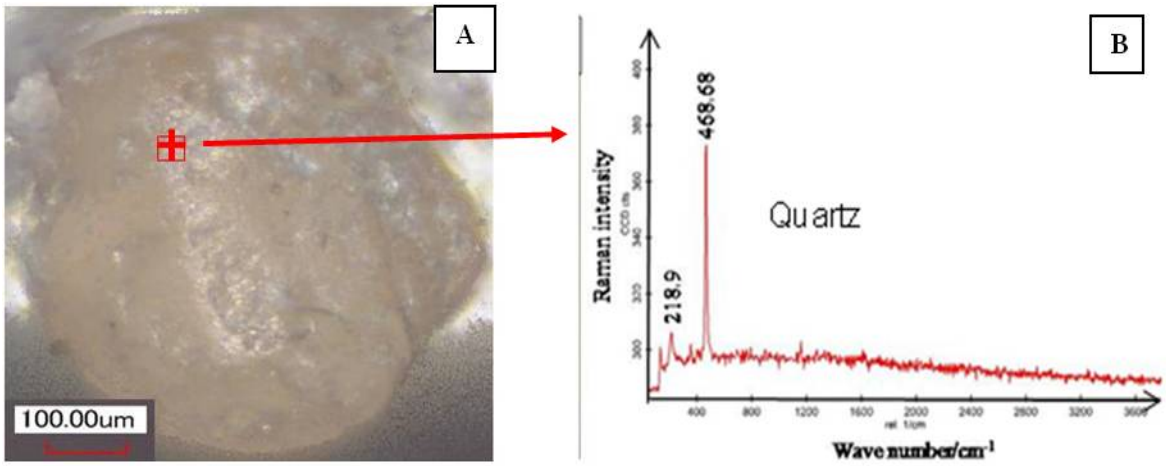

Figure 4.1: Overview image of quartz grain at 5x magnification with binocular and Raman spectrum.

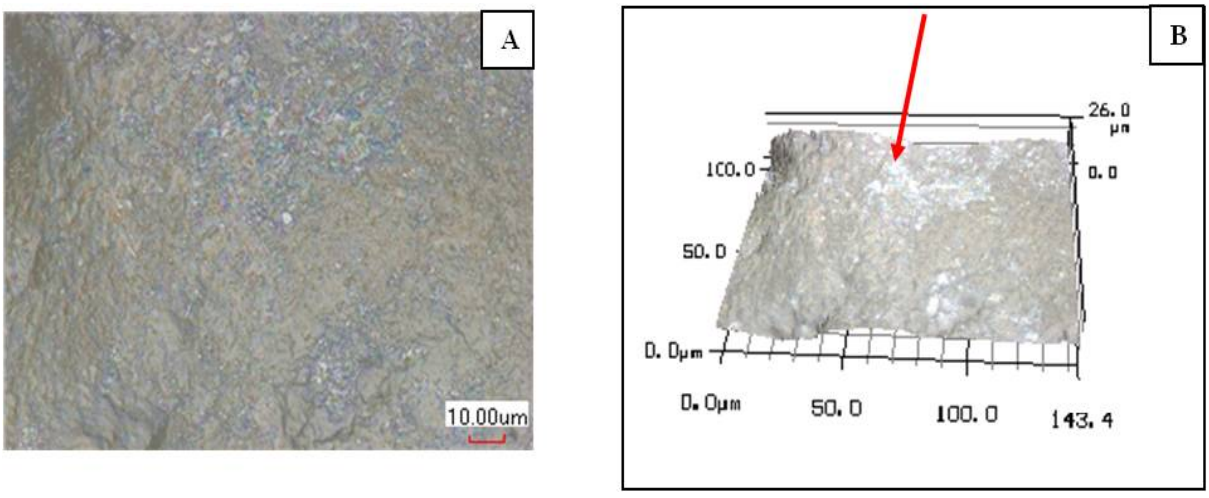

Figure 4.2: CLSM image of the quartz surface taken at 100x magnification.

For many grains taken from the three samples RL I_2111, RL I_4146 and RL I_5042, the roughness was calculated for 50x and 100x magnifications as shown by the root mean square roughness, R_q parameter in table 1.

Table 1: Root mean square roughness R_q parameter calculated at 50x and 100x magnifications

Order	Sample	R_q (µm)		Sample	R_q (µm)		Sample	R_q (µm)	
		50x	100x		50x	100x		50x	100x
1	RL I_2111_1	5.48	2.02	RL I_4146_1	9.9	3.59	RL I_5041_1	9.46	6.12
2	RL I_2111_2	8.53	6.48	RL I_4146_2	5.83	1.87	RL I_5041_2	4.52	1.57
3	RL I_2111_3	5.97	2.52	RL I_4145_3	9.29	9.2	RL I_5041_3	8.22	3.06
4	RL I_2111_4	6.61	4.83				RL I_5041_4	10.09	3.23
5	RL I_2111_5	5.59	5.34				RL I_5041_5	6.83	1.61
6	RL I_2111_6	9.04	2.64				RL I_50441_6	5.22	2.31
7	RL I_2111_7	3.5	2.54				RL I_50441_7	13.02	6.38
8	RL I_2111_8	11.5	3.14				RL I_5041_8	8.72	3.76
9	RL I_2111_9	6.32	3.44						
10	RL I_2111_10	6.27	4.46						
11	RL I_2111_11	9.99	8.25						
12	RL I_2111_12	4.33	2.86						
13	RL I_2111_13	8.59	5.04						
14	RL I_2111_14	13.47	5.32						
15	RL I_2111_15	4.18	3.67						
16	RL I_2111_16	8.99	1.36						

The root mean square roughness R_q depends on the analysed area of the grain surface. At 50x magnification corresponding to a relatively large observation area, the grain surface profile changes in a wide range leading to the large value of R_q. While at 100x magnification (small observation area), the analysed surface area shows more details and finer features can be seen. The grain surface profile only varies in a narrow field, hence leading to small R_q values. As shown in table 1, on the same analysed surface the root mean square R_q at 100x magnification is always smaller than that at 50x magnification for different observation areas. However, decreasing the analysed surface area by a factor of 2 does not decrease R_q by the same factor.

Larger areas show the overview of the surface irregularities (50x), while smaller analysed areas (100x) show more details regarding overgrowth and coating. Therefore, at low magnification grain surfaces with the high root mean square roughness R_q creates rougher pore space than those with low R_q. Otherwise, the analysed surface area at high magnification, the root mean square roughness R_q has been characterised as fractal dimension due to revealing grain surface ruggedness corresponding to numerous curved segments.

As given in table 1, at 50x magnification the grain surfaces of sample RL I_2111 have larger R_q values than of sample RL I_4146 and RL I_5041 which shows the smallest values. It means that pore surfaces of sample RL I_2111 are rougher. While at 50x and 100x magnifications, the R_q values of the grain surfaces of sample RL I_5041 are the smallest that means the pore surfaces are low roughness so the permeability of this sample is the highest. This is consistent with data obtained earlier [5].

The samples RL I_2111 and RL I_4146 with larger R_q values are on the contrary more rough pore surfaces and therefore less permeable.

3.3. Pore space morphology

The morphology of the pores of the investigated reservoir sandstone rocks is characterised by the size of the detrital grains and particularly the grain surfaces as well as growth of authigenic minerals. The primary pore morphology has been modified by both, cementation and authigenic mineral growth in the pores and on the clastic grain surfaces into the pore spaces, these add to the roughness of pores and complicate the pore morphology by protrusions of crystals into the pore space.

In figure 5 a pore space of sample RL I_2111 is filled with precipitated authigenic mineral cement is shown. The mineral has subhedral shape pointing towards albite (confirmed on other samples by EDX and SEM). The surface of the albite has been slightly altered showing small inclusions (rectangles in figure 5A). The minerals surrounding the albite crystal are authigenic calcite cements and/or calcite inclusions (arrows and circle). The albite is displayed in the 3-D image (figure 5B).

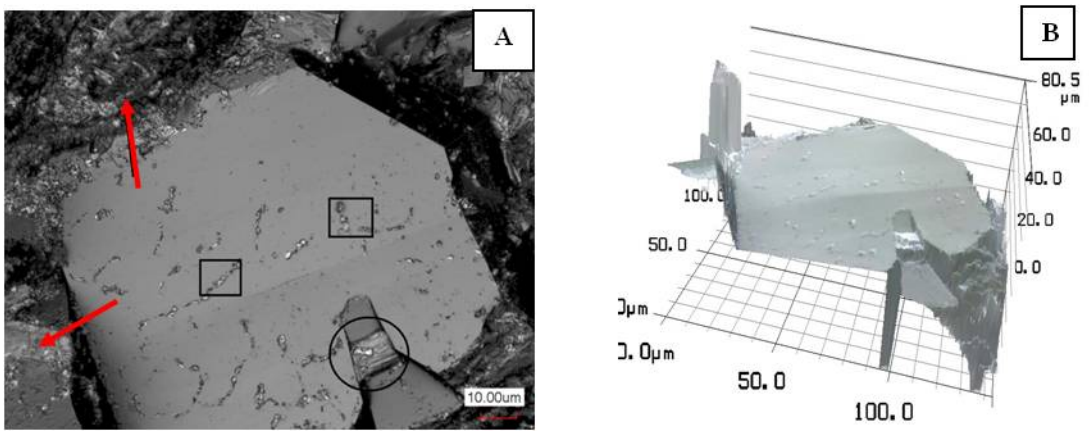

Figure 5: CLSM image taken at 100x magnification showing an albite authigenic mineral grown in the pore space of sample RL I_2111.

The observed pore network in sample RL I_4146, in figure 6 exhibits, that pore geometry is formed and altered due to influence of diagenesis. As can be seen, open pore space is formed by the rhombohedral packing, that detrital grains arrange together forming a triangular pore space (Pore, figure 6.1A) and that the pore is connected to the neighbouring pores by the pore throat (arrow) as shown in the left image (figure 6.1A). Subsequently, the precipitation of calcite cement filled the pores. The calcite cleavage planes are visible in the centre of figure 6.1A and its surface roughness is displayed by the line profile in figure 6.1B. This profile is quite rough with the presence of many high sharp peaks and valleys. In figure 6.2 another pore was drastically altered due to the growth of different authigenic minerals and the dissolution of minerals, on the left hand side (figure 6.2A) albite blades (arrow) are visible. In the centre of the pore needle-shaped crystals of illite (circle) grow into the pore space and overgrow the clastic grain. Some of the needles seem also to have grown from the altered feldspar surface (rectangle), partially this feldspar was dissolved, forming intragranular micro pores.

The profile (figure 6.2B) shows ruggedness of the pore space morphology. Likewise, the pore throats were also altered and narrowed by overgrowth as shown in figures 6.1 and 6.3. In figure 6.3 the pore throat was blocked by cement fill (arrow), this leads to isolated pores forming closed pore spaces and reducing permeability of rocks. In addition, as seen, the grain surface displays micro indention resulting probably from collisions with other grains during transportation or from dissolution during compaction (line mark), in the diagenetic stage authigenic minerals (circle) grew on this surface, which modified the original grain roughness and results in rough pore walls.

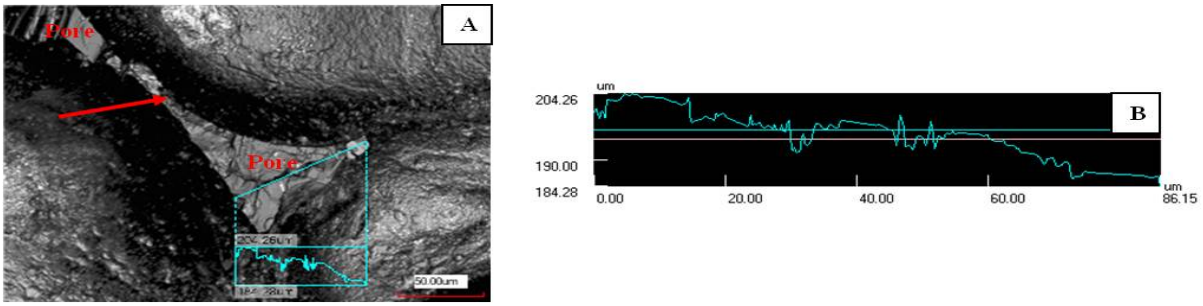

Figure 6.1: CLSM image shows the structure of pore taken at 100x magnification.

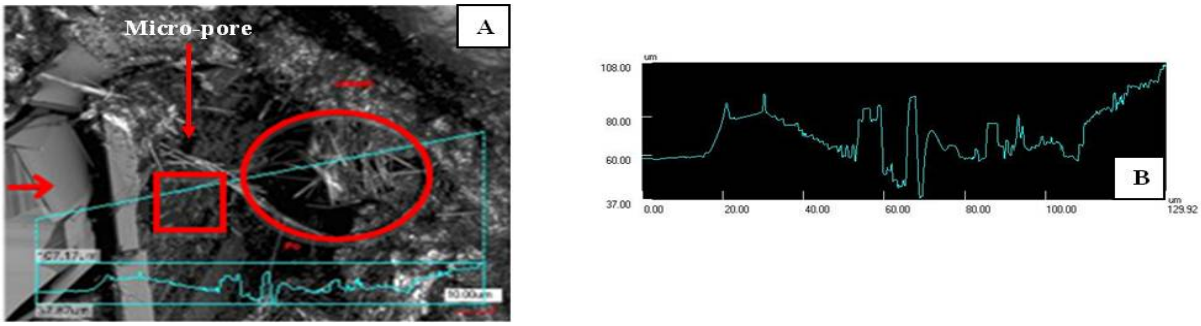

Figure 6.2: An image showing the growth of authigenic minerals in pores taken with CLSM at 100x magnification.

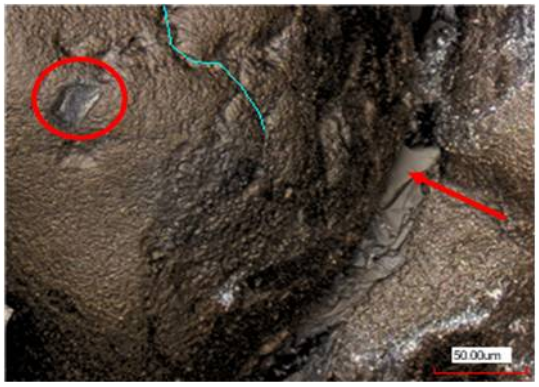

Figure 6.3: Grain surface and pore throat of sample RL I_4146 imaged by CLSM at 50x magnification. The surface of the grain is sculptured by micro-pits (line mark) and overgrown by authigenic minerals (circle). The pore throat is blocked by cement filling (arrow).

The sample RL I_5041 had the highest porosity and the smallest root mean square R_q out of the three investigated samples, as most of the pores seemed to be connected by pore paths, as demonstrated in petrography analysis (figure 1.3). The pore body and pore throats of this sample are shown in the 3-D construction in figure 7. In figure 7.1A the structure of a pore space forms the boundary between grains (G). Some visible apparent illite barriers inside the pore divide the pore space into many micro pores, constructing micro-walls and increasing contact surfaces. The authigenic illite mineral is analysed with SEM (figure 7.1C and D) and EDX spectrum (figure 7.1E). The profile (figure 7.1B) displays the roughness of the pore surface and one of the illite barriers with 17 µm width as marked and thus partly obstructing the flow ability of fluids. The permeability is primarily associated with the porosity, pore sizes and their connectivity to allow the movement of fluids. However, the pore throats connect the open pores in this sample between two grain surfaces which are rather smooth and the pore path width is about 20 µm, as seen in figure 7.2. Thus the potential possible movement of fluids through the pores is much better than in the other samples (see figure 6.3).

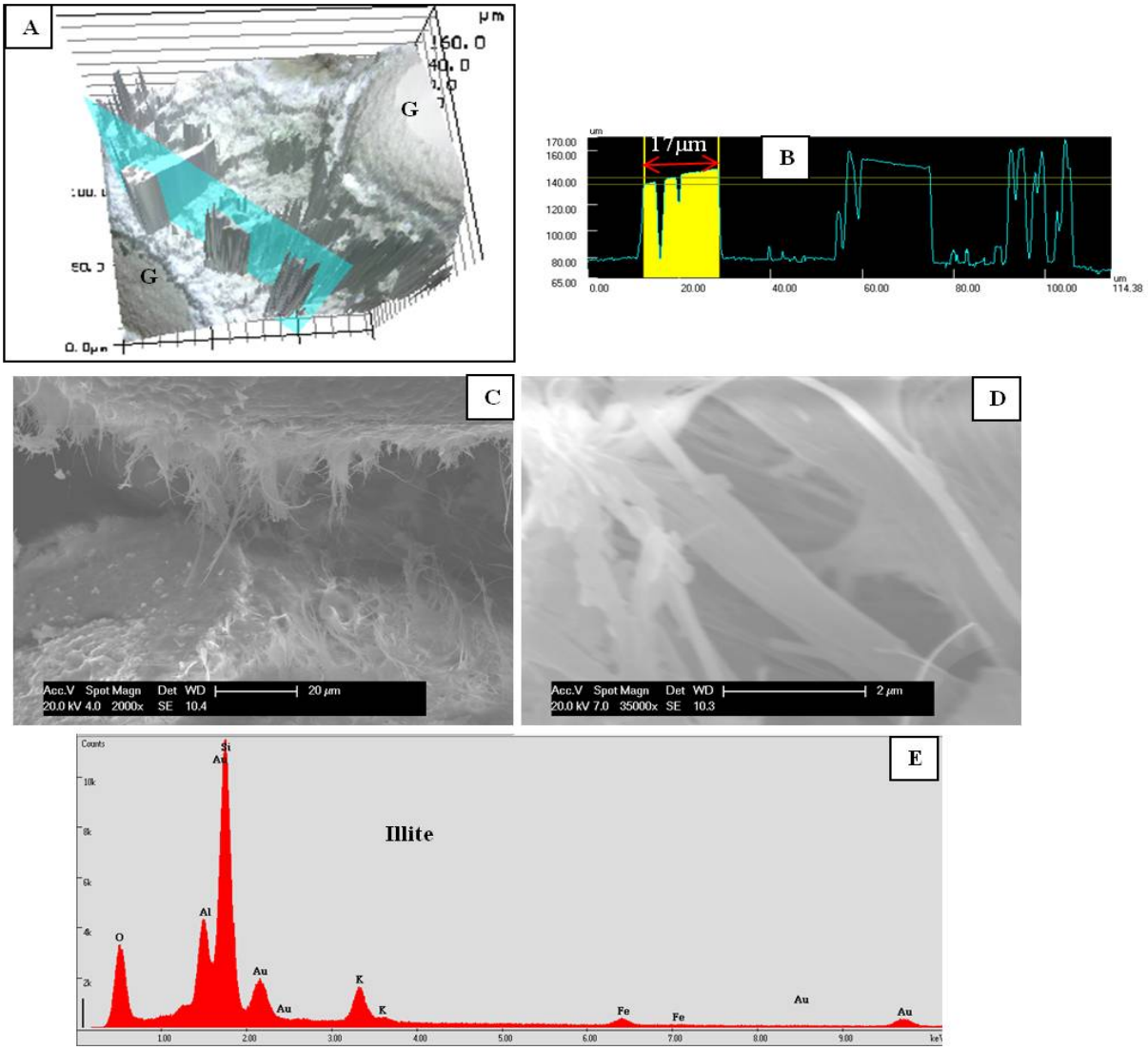

Figure 7.1: CLSM image shows a pore structure in 3-D (A) and in roughness profile (B) of the pore surface. SEM photographs (C and D) display fibrous illites growing into pore and coating on grain surface and EDX spectrum (E).

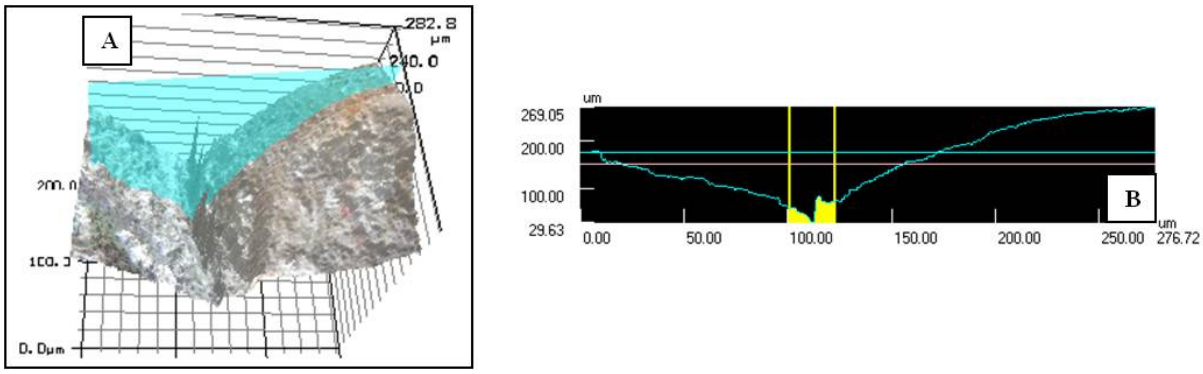

Figure 7.2: CLSM image showing a pore throat.

In brief, the pore characteristics of the investigated sandstone reservoir rocks are associated firstly with the packing of detrital grains; secondly, the alteration of pore geometry through diagenetic processes is most relevant for potential fluid movement. This is demonstrated by the various pore spaces filled by cements, authigenic minerals e.g. in sample RL I_2111, figure 5A. Similarly, in samples RL I_4146 and RL I_5041 the pores are partly cemented by calcite and overgrown by illite and albite, fully or partially blocking the pore throats. Depending on the degree of diagenesis cementation leads to a decrease of the effective porosity and permeability of the sandstone reservoir rocks.

4. Discussion and Conclusions

In the three analysed sandstone samples, the major component is quartz grains with varying, subordinate components of other detrital particles like alkaline feldspar, plagioclase grains and rock fragments. The grain shape is commonly subspheroidal and elongate and the roundness is good. The three samples display a complicated multi phase diagenesis. Primarily, clay minerals are grown in the first stage of diagenesis through grain and matrix alteration. Coatings surrounding grains are generated during further diagenetic stages and are characterised by precipitation of quartz, albite and calcite from fluids, filling the pore spaces, this was also shown in a previous study [10]. Consequently, in the next phase of diagenesis illite replaced albite and feldspar, that formed at the expense of dissolved feldspar (figure 6.2A) at depth in burial diagenesis. In the latest phase calcite cements precipitated from fluid fills into the pore spaces, but overlapping onto quartz cement.

The grain surface topography widely changes during the diagenesis, as observed on the overgrowth of cement and authigenic minerals. This results in grain surfaces with high roughness, as calculated by the root mean square roughness, R_q, parameter.

Equally, the pore geometry was altered depending on the degree of diagenetic alteration. This is demonstrated where the pore space was completely filled by cements, as in sample RL I_2111. Likewise, in samples RL I_4146 and RL I_5041 the pores were partly cemented by calcite and overgrown by illite and albite. Moreover, the pore throats were blocked, therefore, leading to a decrease of the effective porosity and permeability of the reservoir rocks.

The grain roughness analysis at 100x magnification provides detailed characteristics of the grain surface roughness by the root mean square roughness R_q parameter. A comparison of the root mean square roughness R_q values, permeability analysis and fractal dimension D values derived from Small Angle Neutron Scattering Analysis experiments [5] showed good agreements. Small R_q values correspond to a decreased D value and higher permeability. The higher permeability means the fluid flows easily through the rocks. Therefore, the fluid flow through pore spaces of the sample RL I_5041 is less restricted than of the sample RL I_2111 and 4146. Hence, the efficiency of oil exploitation can be reached up high productivity which is extreme important in petroleum industries. These results are an additional step, in further studies of hydrocarbon exploitation of reservoir rocks, tertiary, enhanced recovery methods and CO_2 storage in geological formations. Considerations of the pore morphology and pore roughness down to sub-micron scale and of the varying mineralogy of the pores, are crucial in calculations of the volume of recoverable or hydrocarbons and sequesterable CO_2 quantities.

Acknowledgment

We gratefully acknowledge financial support by the German Federal Ministry of Education and Research (BMBF) for the NanoPorO project FKZ 03G0709A. We thank the Ludwig-Maximilians-University Munich, Department of Earth and Environment Sciences, the Center of Smart Interfaces and the Department of Materials and Geosciences of the Technische Universität Darmstadt, Germany and Analysis Laboratory Center, Vietnam Petroleum Institute (VPI) for supporting the laboratories and carrying this investigation. We also thank RWE Dea AG for providing the samples for our research and for participating in the NanoPorO project and contributing important petrophysical data.

References

[1] Drolon, H., Druaux, F., Faure, A. “Particles shape analysis and classification using the wavelet transform”. Pattern Recognition Letters, vol., 21, pp. 473-482, 2000.

[2] Drolon, H., Hoyez, B., Druaux, F., Faure, A. "Multiscale roughness analysis of particles: Application to the classification of detrital sediments”. International Association for Mathematical Geology, vol., 35, no.7, Oct 2003.

[3] Triolo, F., Triolo, A., Agamalian, M.M., Lin, J-S., Heenan, R.K., Lucido, G., Triolo, R. “Fractal approach in petrology: combining ultra small angle, small angle and intermediate angle neutron scattering”. J. Appl. Cryst, vol., 33, pp. 863-866, 2000.

[4] Sen, D., Mazumder, S., Tarafdar, S. “Pore morphology and pore surface roughening in rocks: a small-angle neutron scattering investigation”. Journal of materials science, vol., 37, pp. 941-947, 2002.

[5] Drobek, T., Strobel, J., Park, S., Lieu, K.P., Altermann, W., Lemmel, H., Lindner, P., Stark, R. W. “Small Angle Neutron Scattering Analysis of Porous Reservoir Rocks”. Internat. Symp. Soc. Core Analysts, Austin, Texas, USA, SCA2011-48, pp. 1-6, Sept. 2011.

[6] Menéndez, B., David, C., Nistal, A.M. “Confocal scanning laser microscope applied to the study of pore and crack networks in rocks”. Computer and Geosciences, vol., 27, pp. 1101-1109, 2001.

[7] Chae, B.G., Ichikawa, Y., Jeong, G.C., Seo, Y.S., Kim, B.C. “Roughness measurement of rock discontinuities using a confocal laser scanning microscope and the Fourier spectral analysis”. Engineering Geology, vol., 72, pp. 181-199, 2004.

[8] Petford, N., Davidson, G., and Miller, J.A. “Pore structure determination using confocal scanning laser microscopy”. Phys. Chem. Earth (A), vol., 24, no.7, pp. 563-567, 1999.

[9] Fredrich, J.T., Greaves, K.H., Martin, J.W. “Pore geometry and transport properties of Fontainebleau sandstone”. Int. J. Rock Mech. Min. Sci and Geomech. Abstr. Vol., 30, No.7, pp. 691-697, 1993.

[10] Altermann, W., Drobek, T., Frei, M., Heckl, W.M., Kantioler, M., Lieu, K.P., Stark, R.W., Strobel, J. "Surface and wetting properties of diagenetic minerals and sedimentary grains in reservoir rocks”. Geotechnologien Science Report, no. 16, pp. 65-75, Oct. 2010.